International Journal of Modern Manufacturing Technologies
ISSN 2067–3604, Vol. XVIII, No. 1 / 2026
https://doi.org/ 10.54684/ijmmt.2026.18.1.97

MANUFACTURING OF ENHANCED RADIATION SHIELDING MATERIALS VIA GREEN SYNTHESIZED NANOPARTICLES

Salam J. Bash Al-Maliki[1], Mohammed S. Al-Maliki[2], Nidaa H. Bash[3], Ali AlMaliki[4], Aya Ahmed[4]

[1]Al-Iraqia University, College of Engineering, Baghdad, Iraq
[2]Middle Technical University, College of Health and Medical Techniques, Baghdad, Iraq
[3]Presidency of the Ministerial Cabinet, Scientific Affairs, Baghdad, Iraq
[4]University of Baghdad, College of Medicine, Baghdad, Iraq

Corresponding author: Mohammed S. Al-Maliki, mohammad.salam@mtu.edu.iq

Abstract: This paper aims to introduce an original green approach for the manufacturing of Copper oxide Nanoparticles (CuO NPs) that have a significant potential to improve the gamma (γ) and X-ray shielding performance of the traditional shielding materials, such as concrete and lead, due to their high density, surface area per unit volume, and high atomic number. The CuO NP additive is synthesised based on algal species, characterised (Field Emission Scanning Electron Microscopy FESEM, Atomic Force Microscopy AFM, X-ray Diffraction XRD, Ultraviolet-Visible Spectroscopy UV, and Fourier Transform Infrared Spectroscopy FTIR), and mixed with the shielding material via ultrasonic mixer to ensure delicate intrusion to the voids and enhancement the final density that is essential for γ-rays and neutrons that are expected in incident radiations. Although the addition of these NPs, 1-2% per cement weight, resulted in a reduction of the concrete compression strength by about 9.8% of its ordinary value, the enhancement of its linear attenuation coefficients (μ) by 29.42% as compared to the original one makes them attractive for nuclear and medical radiation environments. The importance of this approach increases where weight, environmental friendliness, low cost, and long-term radiation durability matter.
Keywords: characterization, green manufacturing, nanomaterial, radiation, shielding.

1. INTRODUCTION

Radioactivity has become an essential component of many modern industries, contributing significantly to advancements in healthcare, energy production, research, and industrial development. Medical imaging technologies such as X-ray and computed tomography (CT), as well as radiotherapy for cancer treatment, rely heavily on controlled sources of ionizing radiation. Similarly, nuclear power plants use radioactive fuel to generate electricity, while industrial sectors such as oil and gas exploration, non-destructive material testing, and scientific research laboratories utilize radioactive sources for measurement, imaging, and analytical purposes, [1, 2]. Although these applications provide undeniable societal benefits, they also introduce potential radiological risks that require careful management.

Protecting individuals from harmful radiation exposure is, therefore, a fundamental concern. While occupational workers operate under regulated exposure limits and monitoring programs, protection of non-occupational individuals demands equally rigorous safeguards. International radiation protection frameworks, particularly those established by the International Atomic Energy Agency (IAEA) and the International Commission on Radiological Protection (ICRP), emphasize three guiding principles: justification of radiation use, optimization of protection, and dose limitation, [3, 4, 5]. For members of the public, the recommended annual effective dose limit is approximately 1 mSv under planned exposure situations. These standards ensure that industrial and medical activities do not pose unacceptable risks to surrounding communities.

Engineering controls form the backbone of public radiation protection. Shielding materials are widely employed to attenuate radiation before it can reach occupied areas. Traditional shielding materials include lead, steel, and concrete, chosen primarily for their high density and atomic number, which enhance their ability to absorb and scatter γ-rays and other forms of ionizing radiation. Concrete is particularly common in nuclear facilities due to its structural strength and relatively low cost. However, conventional materials are not without limitations. Lead, for instance, poses toxicity and environmental concerns, while thick concrete structures can be heavy, bulky, and costly to implement. To address these challenges, researchers have explored the incorporation of additives into shielding materials to improve their performance. Heavy metal oxides such as bismuth oxide (Bi2O3), tungsten

trioxide (WO3), and lead oxide (PbO) have been embedded into polymers, ceramics, and concrete matrices to enhance radiation attenuation. Studies demonstrate that such additives can increase the linear attenuation coefficient and reduce the half-value layer (HVL), meaning thinner or lighter materials can provide equivalent protection, [6, 7, 8]. In addition to performance improvements, some research has focused on developing environmentally friendlier alternatives to traditional lead-based shields.

More recently, nanotechnology has opened new possibilities for radiation shielding enhancement. Nanomaterials, due to their extremely small particle size and high surface area-to-volume ratio, can disperse more uniformly within composite matrices. This uniform distribution increases the probability of interaction between incident radiation and shielding particles. Polymer nanocomposites incorporating Nano-sized bismuth, tungsten, graphene, and silica have demonstrated improved mass attenuation coefficients compared to their micro-scale counterparts, [9, 10]. Furthermore, Nano-additives in high-density concrete have been shown to enhance not only radiation shielding properties but also mechanical strength and durability. Despite promising findings, several challenges remain before Nano-enhanced shielding materials can be widely adopted. Long-term stability under radiation exposure, potential environmental impacts of NPs release, large-scale manufacturing feasibility, and cost considerations must all be addressed. Standardization of testing procedures is also necessary to allow consistent comparison between the relevant materials, [11].

In recent years, researchers have increasingly explored the use of NPs to improve the performance of radiation shielding materials. Traditional shielding materials such as lead and heavy concrete are effective but often bulky and environmentally problematic. By contrast, incorporating NPs into polymers and cement-based matrices offers a promising way to achieve comparable or improved radiation attenuation with reduced weight and greater material flexibility, [12, 13]. The improvement in shielding performance arises largely from the unique properties of NPs. Because of their extremely small size and high surface-to-volume ratio, NPs disperse more uniformly within a host material than conventional micro-sized fillers. This uniform distribution reduces internal voids and increases the likelihood of photon–matter interactions. When high-atomic-number (high-Z) NPs such as bismuth oxide (Bi_2O_3) or lead oxide (PbO) are used, the probability of photoelectric absorption and Compton scattering increases significantly, particularly within diagnostic and therapeutic photon energy ranges, [14, 15]. Polymer-based nanocomposites have been widely investigated in this context. Studies show that epoxy systems reinforced with NPs such as Sb_2O_3, Al_2O_3, Bi_2O_3, and SnO_2 exhibit higher linear attenuation coefficients than unmodified polymers, [16]. Similarly, polystyrene composites containing PbO NPs demonstrated 22–30% greater mass attenuation compared to similar composites filled with micron-scale PbO particles, highlighting the advantages associated with nanoscale dispersion, [17]. These findings suggest that the nanoscale dimension of the fillers enhances the effective interaction cross-section, thereby improving shielding efficiency without proportionally increasing material thickness. NPs incorporation has also been examined in structural and cementitious materials. For example, polypropylene and cement composites doped with Fe_3O_4 or CdO NPs showed improved attenuation of both γ-rays and neutrons compared to conventional formulations, [18]. However, researchers have noted that increasing the NPs content can influence mechanical strength, density, and porosity. As a result, optimizing filler concentration is essential to maintain structural performance while maximizing radiation attenuation. Advances in additive manufacturing have further expanded the design possibilities for NPs-enhanced shields. Three-dimensional printed polylactic acid materials embedded with bismuth NPs achieved superior mass attenuation relative to bulk filler systems, demonstrating how controlled geometry and nanoscale dispersion can work together to improve performance, [15]. Such developments point toward customizable, lightweight shielding solutions suitable for medical imaging rooms, nuclear facilities, and portable protective equipment. Overall, current research consistently indicates that NPs-reinforced composites can significantly enhance radiation attenuation while reducing weight and improving material versatility. Continued investigation is needed to address long-term stability, cost considerations, and mechanical optimization, but the evidence supports nanotechnology as a promising direction in next-generation radiation shielding materials.

The main goal of this paper is to determine the potential of incorporating synthesised CuO NPs based on green algae as an additive to conventional concrete, on the latter's radiation attenuation capability and other mechanical properties.

2. MATERIALS AND METHODS

The goal of this study is a three-fold mission: synthesis of CuO NPs, mixing of the NPs with a conventional concrete constituent, and testing the produced concrete slab against a radioactive source to determine its attenuation coefficient and compare it with that of the conventional concrete slab. The synthesis method involves using 100 ml of Cladophora glomerata algal extract (obtained from the postgraduate studies laboratory at the Faculty of Biological Sciences, University of Baghdad) to dissolve 10 g of $Cu(NO_3)_2$. The mixture was then stirred

for 8 hours at 120 rpm. The product was centrifuged for 20 minutes at 4000 rpm and then separated to remove the upper liquid phase from the residue powder, which was washed three times with 99% ethanol and dried at 40 °C in petri dishes. Characterization of the synthesized CuO NPs is an essential step to ensure the production success. The concrete slab was made via the application of normal-weight aggregates per ASTM C33, ready-mix per ASTM C94); Coarse Aggregate 45–55%, Sand 25–35%, Portland cement 10–15%, and Water 5–8%, then left 28 days to dry, then tested for the mechanical properties and the radioactivity attenuation ability. The aforementioned synthesized CuO NPs were added as 5, and 10% of the cement weight to the above mixture via the use of Ultrasonic Homogenizer LX101UH to avoid any possible agglomeration. The enhanced concrete slab would be ready to test the new mechanical properties and the radioactivity attenuation ability as represented by the linear attenuation coefficients (μ) and energy reduction according to the following equation (1):

$$\mu = \frac{1}{x} \ln \frac{I}{I_0} \tag{1}$$

where: I/I_0 : radiation intensity after, and before the concrete sample; x: thickness of sample.

3. RESULTS AND DISCUSSION

Samples of the algal extract from the cultivated *Cladophora glomerata* green algae were prepared following the aforementioned procedure. This extract was mixed and stirred with blue $Cu(NO_3)_2$ solution, as previously described. The resulting light green powdered NPs were obtained by centrifugation, indicating the initial formation of CuO NPs.

The morphology of the produced NPs was characterized using the Field Emission Scanning Electron Microscopy (FESEM) test to check the microstructure of the synthesized NPs and their surface morphology. The results demonstrated the quasi-spherical shape of the produced CuO NPs of 40.15-66.09 nm diameter that tend to agglomerate in cluster-like formations because of their remarkable surface energy and bioorganic content of the utilized extract of the *Cladophora glomerata* algae. The observed agglomeration was a consequence of both the drying processes, whether naturally or via incubation, preparation, and inter-particle interactions.

The results of the Atomic Force Microscopy (AFM) characterization test showed strong consistency with those of the FESEM test. The quasi-spherical shape of the NPs (with an average diameter of 58.18 nm, compared to the approximated average particle diameter of 58.10 nm from the FESEM test) was distributed uniformly and does not have sharp edges (Figure 1). Additionally, the moderate roughness of the particle surfaces was indicated by the root mean square roughness (RMS) of the coated surfaces, which was measured by AFM as 70.06 nm, and the average roughness was 45.43 nm.

The X-ray Diffraction (XRD) test was achieved using the diffractometer with the specifications shown in Table 1. This test serves to examine the phase purity and crystalline structure of the synthesized CuO NPs. Data were collected from position angles (2θ) of 8° to 100°, capturing the characteristic reflections of monoclinic CuO.

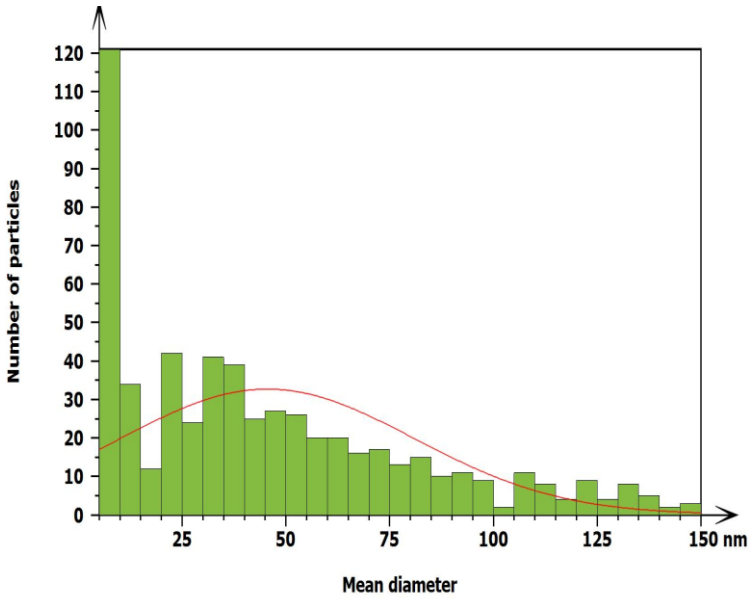

Fig. 1. Particle analysis of the synthesized CuO NPs via AFM test

Table 1. The technical specifications of the diffractometer used for the XRD tests

Brand	*Bruker*
Model	D2 PHASER
Scan Range (2θ)	~5° – 115°
Cu-Kα radiation λ	~1.5406 Å

The obtained diffraction form is shown in Figure 2 (red curve). The most intense reflection appears at 35.5°, corresponding to the (-111) and (111) crystal planes; the dominant orientations for this phase. Additional peaks are clearly visible at 32.5°, 38.7°, 48.8°, 53.5°, 58.3°, 61.5°, 66.2°, and 68.1°, all matching the monoclinic CuO structure. To verify the phase identification, a comparison between the experimental data and the monoclinic CuO reference (ICDD PDF Card No. 96-900-8962, black curve) [20] was included in Figure 3. The overlay confirms excellent agreement in peak positions. Every significant reflection in the tested sample lines up with a peak in the reference card, and no unidentified peaks appear. This confirms that the synthesised NPs are phase-pure monoclinic CuO, free from impurities like Cu_2O or metallic copper. Additionally, the sharp peaks indicate good crystallinity, though some broadening is visible. This is expected for nanomaterials and likely comes from small crystallite size rather than lattice strain, [21, 22].

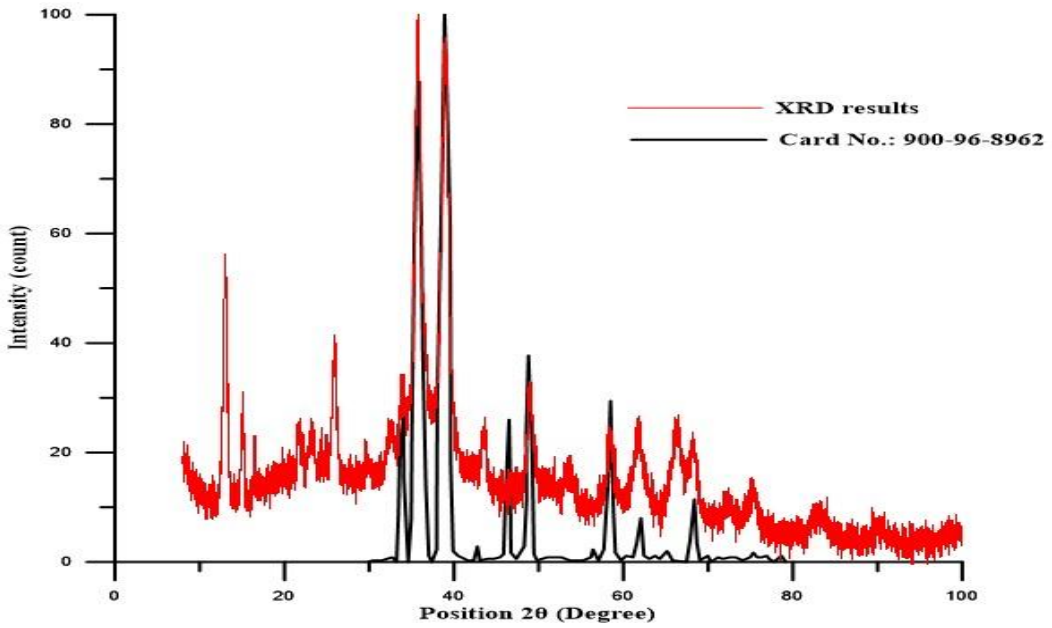

Fig. 2. Normalized XRD curve of synthesized CuO NPs (black line) compared with the monoclinic CuO reference pattern (ICDD PDF Card No. 96-900-8962, red line)

The optical characteristics of the CuO NPs were determined via the Ultraviolet-Visible Spectroscopy (UV-vis) spectrophotometer (specifications were listed in Table 2), in addition to their band gap. The results revealed three non-overlapping, or in other words, distinct peaks of absorption at approximately 297, 299, and 304 nm, corresponding to multiple optical transitions linked to various organizational and/or electronic characteristics of the NPs. The first two approximately equal peaks were attributed to the confined NPs that have smaller sizes [23], while the third one was attributed to the larger-sized particles. These peaks suggest the semi-heterogeneous regime in the states of the surface within the NPs, [24].

Table 2. The technical specifications of the spectrophotometer used for the UV-vis test

Brand	*Bruker*
Model	LAMBDA 365, Double-Beam Spectrophotometer
Wavelength Range	190 – 1100 nm
Quartz Cuvette Path Length	Standard cell holder (10 mm)

The final characterization test was the Fourier Transform Infrared Spectroscopy (FTIR) test, the results of which were shown in Figure 3. The analysis of this figure was based on the observed peaks and their corresponding

locations. The FTIR spectrum reveals strong Cu–O peaks before 800 cm^{-1}, weak organic-related peaks, and the low O–H stretching that was attributed to adsorbed water, these confirm the success of the green algal synthesis of highly pure CuO NPs.

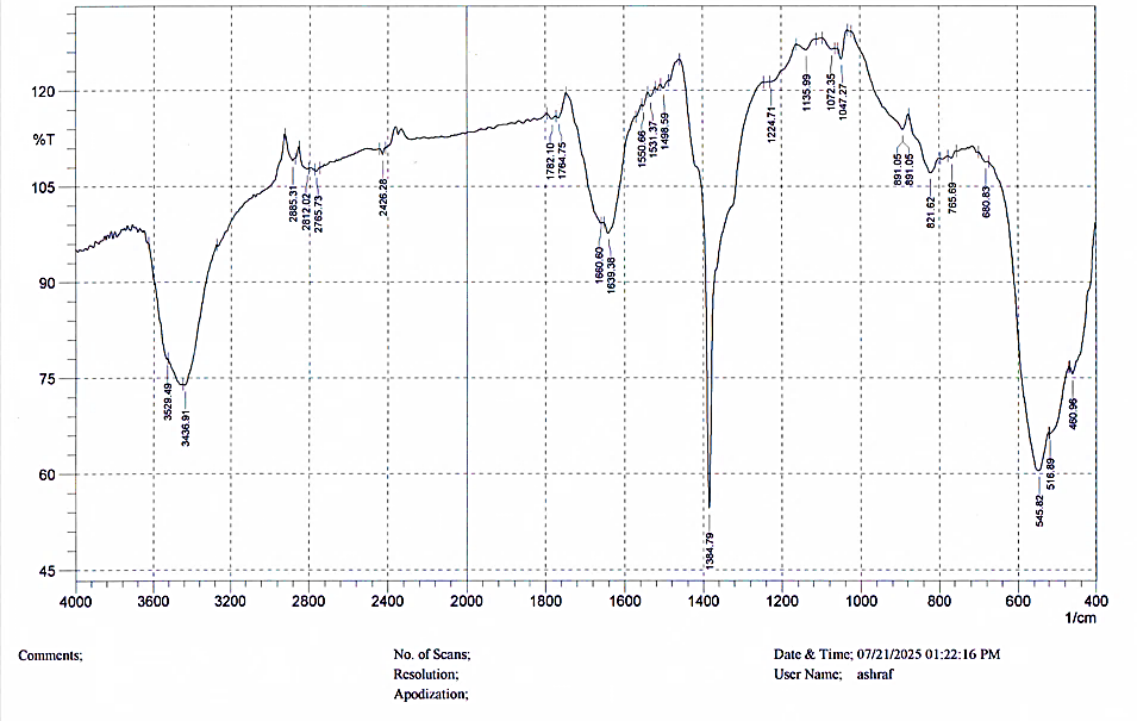

Fig. 3. FTIR diagram for the synthesized CuO NPs

The compressive strength tests for conventional concrete specimens and these with the CuO NPs additives are demonstrated in Table 3. The compressive strength tests show that adding NPs significantly affects the mechanical performance of concrete, with the effect strongly dependent on the number of NPs added. All specimens had a cross-sectional area of 2500 mm^2, and testing was consistent across all specimens. For the conventional concrete; 0% NPs, the measured compressive stresses were 20.23 MPa, 19.78 MPa, and 20.35 MPa, resulting in an average of 20.12 MPa. The small variation indicates reliable specimen preparation and consistent testing. With 5% CuO NPs by cement weight, the compressive stresses increased markedly to 25.784 MPa, 25.692 MPa, and 25.780 MPa, respectively, averaging 25.75 MPa. This 28% improvement over the conventional concrete is likely due to the NPs acting as fine fillers, reducing micro-voids, providing nucleation sites for cement hydration products such as calcium silicate hydrate (C–S–H), and improving the interfacial transition zone between paste and aggregates. At 10% CuO NPs addition, compressive stresses were 21.172 MPa, 21.244 MPa, and 21.288 MPa, averaging 21.24 MPa. While slightly higher than the conventional mix, this is a noticeable decrease from the 5% mixture. The reduced strength at higher NP content is attributed to particle agglomeration, partial cement replacement reducing hydration, and decreased workability, leading to higher porosity.

Table 3. The compression stress for various concrete mixtures

Area (mm^2)	Load (kN)	Stress (MPa)	Avg. Stress (MPa)	CuO NPs Addition
2500	50.575	20.23	20.12	0%, Conventional concrete
	49.450	19.78		
	50.875	20.35		
	64.460	25.784	25.75	5% by cement weight
	64.230	25.692		

Area (mm²)	Load (kN)	Stress (MPa)	Avg. Stress (MPa)	CuO NPs Addition
	64.450	25.780		
	52.930	21.172		
	53.110	21.244	21.24	10% by cement weight
	53.220	21.288		

The γ-ray shielding performance of concrete specimens containing different amounts of CuO NPs (0%, 5%, and 10% by weight of cement) was investigated using a Cs-137 radioactive source emitting 662 keV γ-rays. The concrete specimens had cross-sectional dimensions of 8 × 8 cm and were tested at thicknesses of 1 cm and 2 cm. The results are demonstrated in Table 4. The results show a clear increase in the μ values with higher CuO NPs content as 0% CuO yielded μ value of 0.17 cm^{-1}, 5% CuO NPs increased this to 0.21 cm^{-1}, and 10% CuO NPs achieved the highest value of 0.22 cm^{-1}. This trend indicates that incorporating CuO NPs enhances the material's ability to attenuate γ-radiation. The improvement can be attributed to the higher atomic number and density contribution of CuO NPs, which increases the likelihood of photon interactions such as Compton scattering and photoelectric absorption within the concrete. Energy transmission measurements further confirm these observations. For 1 cm thick specimens, the transmitted energy was 84.37% for conventional concrete, 81.06% for 5% CuO, and 80.25% for 10% CuO NPs. Doubling the thickness to 2 cm reduced the transmitted energy to 71.18%, 65.70%, and 64.40% for the same respective specimens. These results illustrate that both increasing the CuO NPs content and the specimen thickness significantly improve gamma-ray attenuation, consistent with the Beer–Lambert law, where transmitted intensity decreases exponentially with material thickness and its attenuation coefficient.

Table 4. Linear Attenuation Coefficient for CuO NPs-Concrete sample

CuO NPs %	μ (cm^{-1})	Transmitted Energy (Thickness of 1 cm) %	Transmitted Energy (Thickness of 2 cm) %
0	0.17	84.367	71.18
5	0.21	81.06	65.705
10	0.22	80.252	64.44

4. CONCLUSIONS

Industries involving radioactivity play a vital role in modern society, yet they require strict and carefully engineered protective measures to safeguard non-occupational populations. While traditional shielding materials remain effective and widely used, ongoing research into composite additives and nanomaterials offers promising advancements toward lighter, safer, and more efficient radiation protection systems. The tests regarding the addition of various amounts of green-based synthesized CuO NPs to a conventional concrete mixture suggest that the incorporation of NPs can enhance compressive strength when used at an optimal percentage. Based on the present findings, 5% CuO NP addition appears to be more effective than 10%, providing improved mechanical performance without the negative effects associated with higher amounts. Future investigations involving microstructural analysis would help further explain the interaction between CuO NPs and cement hydration products. The findings of the radiation shielding tests regarding the inclusion of CuO NPs demonstrate that CuO NPs can effectively enhance the γ-rays shielding properties of concrete in a dosage-dependent manner. A 5% addition of CuO NPs provides substantial improvement in attenuation without likely affecting the concrete's workability, while 10% offers slightly greater shielding. This suggests that CuO-modified concrete can be a practical solution for improving radiation protection, particularly against medium-energy γ-sources like Cs-137. Future studies using microstructural analysis could provide further insights into the distribution of NPs and their interactions with γ-radiation within the concrete matrix. Continued interdisciplinary research will be essential to ensure that technological progress in radioactive applications is matched by equally robust advancements in public safety.

Author contributions: The conceptualization, methodology, and overall guidance of this study were primarily carried out by SJBAM, MSAM. The experimental work, including calculations, tabulation, and data representation, was jointly conducted by NHB, AAM, AA. All authors contributed to the writing, revision, and final approval of the manuscript.

Funding: This paper has received no external funding.

Conflicts of interest: There is no conflict of interest.

5. REFERENCES

[1]. International Atomic Energy Agency. (2018). *IAEA at work: 2018 edition*. International Atomic Energy Agency. https://www.iaea.org/sites/default/files/18/09/iaea-at-work-2018.pdf

[2]. U.S. Nuclear Regulatory Commission. (2023). *Uses of radiation*. U.S. Nuclear Regulatory Commission. https://www.nrc.gov/about-nrc/radiation/around-us/uses-radiation.html

[3]. International Atomic Energy Agency. (2014). *Radiation protection and safety of radiation sources: International basic safety standards (General Safety Requirements Part 3, No. GSR Part 3)*. IAEA. https://www.iaea.org/publications/8930/radiation-protection-and-safety-of-radiation-sources-international-basic-safety-standards

[4]. Al-Maliky S. J. B., AlKhayat Z. Q. (2012). *Kitchen food waste inventory for residential areas in Baghdad City*. Modern Applied Science, 6(8), 45–51. https://doi.org/10.5539/mas.v6n8p45.

[5]. International Commission on Radiological Protection. (2007). *The 2007 recommendations of the International Commission on Radiological Protection (ICRP Publication 103)*. Elsevier. https://doi.org/10.1016/j.icrp.2007.10.003

[6]. Al-Saleh W. M., Almutairi H. M., Sayyed M. I., Elsafi M. (2023). *Multilayer radiation shielding system with advanced composites containing heavy metal oxide nanoparticles: a free-lead solution*. Scientific Reports, 13(1), 18429. https://doi.org/10.1038/s41598-023-45621-2

[7]. Elisha E., Maliki S. J. B., Abraham, B. K. (1988). *Effects of Jasminum officinale flowers on the central nervous system of the mouse.* International Journal of Crude Drug Research*, 26*, 221–226. https://doi.org/10.3109/13880208809053923

[8]. Elsafi S., Sayyed M. I., Al-Qaradawi S. Y., Almuqrin A. H. (2023). *Development of novel nanocomposite radiation shielding blocks as gamma rays barrier*. Radiation Physics and Chemistry, 212, 111116. https://doi.org/10.1016/j.radphyschem.2023.111116

[9]. Kassim H., Aldawood S., Prasad S., Asemi N. N., Aziz A. A., AlSalhi M. S. (2024). *Advanced polymeric matrix utilizing nanostructured bismuth and tungsten oxides for gamma rays shielding*. Heliyon, 10(17), e37289. https://doi.org/10.1016/j.heliyon.2024.e37289.

[10]. Yılmaz M., & Akman F. (2023). *Gamma radiation shielding properties for polymer composites reinforced with bismuth tungstate in different proportions*. Applied Radiation and Isotopes, 200, 110994. https://doi.org/10.1016/j.apradiso.2023.110994.

[11]. Pomaro B. (2016). *Radiation damage in concrete structures*. Cement and Concrete Research, 85*,* 1–11. https://doi.org/10.1016/j.cemconres.2016.03.012.

[12]. Abouhaswa A. S., Sayyed M. I., Al-Ghamdi A. A., Elsafi M. (2023). *The use of nanomaterial polymeric materials as ionizing radiation shields*. Radiation Physics and Chemistry, 206, 110843. https://doi.org/10.1016/j.radphyschem.2023.110843

[13]. Shahzad K., Kausar A., Manzoor S., Rakha S. A., Uzair A., Sajid M., Arif A., Khan A. F., Diallo A., Ahmad I. (2023). *Views on radiation shielding efficiency of polymeric composites/nanocomposites and multi-layered materials: Current state and advancements*. Radiation, 3(1), 1–20. https://doi.org/10.3390/radiation3010001.

[14]. Said A. M., Zeidan M. S., Bassuoni M. T., Tian Y. (2012). *Properties of concrete incorporating nano-silica*. Construction and Building Materials, 36, 838–844. https://doi.org/10.1016/j.conbuildmat.2012.06.044.

[15]. Li H., Xiao H. G., Yuan J., Ou J. (2004). *Microstructure of cement mortar with nano-particles.* Composites Part B: Engineering, 35(2), 185–189. https://doi.org/10.1016/S1359-8368(03)00052-0.

[16]. Gouda M. M., Abbas M. I., Hammoury S. I., Zard K., El-Khatib A. M. (2023). *Nano tin oxide/dimethyl polysiloxane reinforced composite as a flexible radiation protecting material*. Scientific Reports, 13, 210. https://doi.org/10.1038/s41598-023-27464-z.

[17]. Elsafi M., El-Nahal M. A., Sayyed M.I., Saleh I. H., Abbas M. I. (2022). *Novel 3-D printed radiation shielding materials embedded with bulk and nanoparticles of bismuth*. Scientific Reports, 12(1), 12467. https://doi.org/10.1038/s41598-022-16317-w.

[18]. Salah A. A., El-Khatib A. M., Shalaby T. I., Elsafi M. (2024). *Shielding performance of metal oxide nanoparticles-doped polypropylene composites against gamma rays and neutrons exposure*. Radiation Physics and Chemistry, 216, 111461. https://doi.org/10.1016/j.radphyschem.2023.111461.
[19]. Hubbell, J.H. Seltzer, S.M. (1995). *Tables of X-Ray Mass Attenuation Coefficients and Mass Energy-Absorption Coefficients 1 keV to 20 MeV for Elements Z = 1 to 92 and 48 Additional Substances of Dosimetric Interest.* National Institute of Standards and Technology (NIST), NIST IR 5632. https://doi.org/10.6028/NIST.IR.5632
[20]. International Centre for Diffraction Data (ICDD), PDF Card No. 96-900-8962 (CuO, Tenorite), (2024).
[21]. Dubey, R.S., Rajesh, Y.B.R.D., More, M.A. (2015). *Synthesis and characterization of SiO2 Nanoparticles via sol-gel method for industrial applications*. Materials Today: Proceedings, 2(4-5), 3575-3579. https://doi.org/10.1016/j.matpr.2015.07.098.
[22]. Smith B. C. (2011). *Fundamentals of Fourier Transform Infrared Spectroscopy (2nd ed.).* CRC Press, Taylor & Francis Group, Boca Raton, London, New York.
[23]. Khalil Z., Hummadi K. (2025). *Nano-silica oxide modified porcelanite for enhanced adsorption of levofloxacin from aqueous solution.* International Journal of Design & Nature and Ecodynamics, 20(8), 1745–1758. https://doi.org/10.18280/ijdne.200806.
[24]. Turtogtokh E., Tsermaa G. (2023). *Sol-Gel synthesis and optical characterization of ZnO nanoparticles*. Materials Science Forum, 1083, 70–74. https://doi.org/10.4028/p-7e2ilq.

Received: March 30th, 2026 / Accepted: June 15th, 2026 / Paper available online: June 20th, 2026 © International Journal of Modern Manufacturing Technologies.